Check for updates

Ni nanocatalysts supported on mesoporous Al_2O_3–CeO_2 for CO_2 methanation at low temperature†

Yushan Wu, [ID] [a] Jianghui Lin, [a] Guangyuan Ma, [a] Yanfei Xu, [a] Jianli Zhang, [b] Chanatip Samart [c] and Mingyue Ding [ID] ⋆[abd]

The selectivity and activity of a nickel catalyst for the hydrogenation of carbon dioxide to form methane at low temperatures could be enhanced by mesoporous Al_2O_3–CeO_2 synthesized through a one-pot sol–gel method. The performances of the as-prepared Ni/Al_2O_3–CeO_2 catalysts exceeded those of their single Al_2O_3 counterpart giving a conversion of 78% carbon dioxide with 100% selectivity for methane during 100 h testing, without any deactivation, at the low temperature of 320 °C. The influence of CeO_2 doping on the structure of the catalysts, the interactions between the mesoporous support and nickel species, and the reduction behaviors of Ni^{2+} ions were investigated in detail. In this work, the addition of CeO_2 to the composites increased the oxygen vacancies and active metallic nickel sites, and also decreased the size of the nickel particles, thus improving the low temperature catalytic activity and selectivity significantly.

1 Introduction

Natural gas is a potential clean fuel as well as an important feedstock used to produce other key industrial chemicals. The process of carbon dioxide (CO_2) hydrogenation to produce methane (CH_4) is a promising route for recycling CO_2 captured from the combustion of fossil fuels.[1–4] CO_2 methanation, also known as the Sabatier reaction ($4H_2 + CO_2 \rightarrow CH_4 + 2H_2O$, $\Delta H_{298\ K} = -165$ kJ mol^{-1}), is exothermic and thermodynamically favoured at low temperatures but there are significant kinetic barriers[5] and thus it still remains a big challenge to develop a catalyst with both excellent catalytic activity and selectivity at low temperatures. Great efforts have been made to study metal-supported catalysts for the hydrogenation of CO_2 to CH_4. Compared with expensive noble metals (Rh, Ru, Pd) and other common transition metals (Fe, Co),[6–11] Ni-based composites, so far, have been the most extensively used in CO_2 hydrogenation to CH_4 because of their low cost, excellent catalytic activities and selectivity.[12–16] However, the sintering problems of Ni nanoparticles at relatively high reaction temperatures and the deposition of carbon lead to rapid deactivation during the reaction processes.[17] Therefore, it is desirable to explore novel nanocatalysts which are highly efficient, mechanically resistant, chemically and physically stable, and resistant to sintering.

Many strategies have been proposed to alleviate the fast deactivation and low selectivity of catalysts for CH_4, such as the modification of catalytic supports, the addition of structural or electronic promoters, and adjustments to the preparation routes for the catalysts.[18–23] Among these, the modification of supports has drawn much attention because changes to the metal-support interactions affect the reactivity and bonding of chemisorbed molecules as well. For instance, MgO and ZrO_2 were investigated for their capacities to improve the catalytic activity and selectivity of heterogeneous catalysts.[24–27] In general, CeO_2 has acted as an electronic and structural promoter to enhance the performance of Ni-based catalysts by reinforcing the thermal stability, and improving the exchange of oxygen species as well as the uniform distribution of metals over the catalyst.[28–30]

Here, we describe a Ni-modified catalyst loaded on an Al_2O_3–CeO_2 support through a one-pot sol–gel method, and demonstrate its activity for the hydrogenation of CO_2. The increased quantity of active nickel sites combined with the oxygen vacancies of the composite support promoted by CeO_2 lead to an excellent performance in the hydrogenation of CO_2 to form CH_4. Although there are some reports in the literature regarding CeO_2-based composites for CO_2 methanation, most of these have used CeO_2 as a separate carrier or promoter, and very few reports have focused on the Ce species as both a promoter and a carrier at the same time. The low content of Ce and the poor interaction between CeO_2 and Al_2O_3 in composites prepared in previous studies have led to inferior catalytic performance.[31–33]

[a] School of Power and Mechanical Engineering, Hubei International Scientific and Technological Cooperation Base of Sustainable Resource and Energy, Hubei Province Key Laboratory of Accoutrement Technique in Fluid Machinery & Power Engineering, Wuhan University, Wuhan 430072, China. E-mail: Dingmy@whu.edu.cn

[b] State Key Laboratory of High-efficiency Utilization of Coal and Green Chemical Engineering, Ningxia University, Yinchuan 750021, China

[c] Department of Chemistry, Faculty of Science and Technology, Thammasat University, Rangsit Campus, Klongluang, Pathumtani 12120, Thailand

[d] Shenzhen Research Institute of Wuhan University, Shenzhen 518108, China

† Electronic supplementary information (ESI) available. See DOI: 10.1039/c9ra08967e

In this study, we have developed a mild method to construct Al_2O_3–CeO_2 composites, namely a one-step sol–gel method. These Al_2O_3–CeO_2 composites have high redox activity, high numbers of oxygen vacancies, resistance to sintering and excellent thermal stability. Our Al_2O_3–CeO_2-1.0-supported Ni catalyst exhibited 100% selectivity for CH_4 with 78% CO_2 conversion in a 100 h test at the low temperature of 320 °C.

2 Experimental section

2.1 Preparation of catalysts

$Al(NO_3)_3 \cdot 9H_2O$ (99.99%), $Ce(NO_3)_3 \cdot 6H_2O$ (99.99%) and $Ni(NO_3)_3 \cdot 6H_2O$ (99.99%) were purchased and used without further purification. A series of Ni-supported mesoporous Al_2O_3–CeO_2 composites with different Al/Ce ratios (1 : 0, 10 : 1, 5 : 1, 2.5 : 1 and 1 : 1) were prepared via a one-pot sol–gel route.[34] Briefly, $Ce(NO_3)_3 \cdot 6H_2O$ (7.5 g, 0.02 mol) and $Al(NO_3)_3 \cdot 9H_2O$ (8.68 g, 0.02 mol) were dissolved in 50 mL EtOH, and a moderate amount of $Ni(NO_3)_3 \cdot 6H_2O$ (2.46 g, 8 mmol) was added to the solution with vigorous stirring. Then 1,2-epoxypropane (25 mL) was added dropwise to the above solution with stirring until gels formed. After being aged at room temperature for 48 h, the gels were five times solvent exchanged with EtOH to remove impurities, and dried at 80 °C for two days. The white product Ni/Al_2O_3–CeO_2-1.0 (Al/Ce mole ratio = 1) was obtained by calcining the powder at 500 °C for 7 h. In the composites, the sum mole ratio of Al and Ce was fixed at 0.04 mol, and the Ni content was maintained at 10 wt%. The resulting porous 10Ni/Al_2O_3–CeO_2 catalysts were named Ni/Al_2O_3–ZrO_2-x (x = 10, 5.0, 2.5, and 1.0), where x represents the Al/Ce ratio. Single Ni/Al_2O_3 catalysts were prepared for comparison using the same process but without adding the Ce source.

2.2 Material characterizations

X-ray Photoelectron Spectroscopy (XPS) was conducted on an ESCALAB250Xi XPS spectrometer (Thermo Fisher Scientific), and the binding energies of all photoelectron peaks were calibrated using C 1s spectra (binding energy at 284.8 eV). Powder X-ray Diffraction (PXRD) characterization was performed on a Smartlab diffractometer (Rigaku) with filtered Cu Kα radiation (λ = 1.5405 Å). N_2 adsorption and desorption isotherms were performed on an Autosorb iQ2 analyzer (Quantachrome) in a liquid nitrogen bath at 77 K. H_2-temperature programmed reduction (H_2-TPR) was conducted using an Altamira AMI 200-R-HP unit with a thermal conductivity detector (TCD). Thermogravimetric analysis (TGA) was performed on a DTG-60 thermal gravimetric analyser (Shimadzu) in an air atmosphere. All prepared catalysts were stored in an inert glovebox (O_2 < 0.1 ppm, H_2O < 0.1 ppm, Mikrouna) before use and characterization.

2.3 Catalytic tests

CO_2 methanation was performed in a continuous fixed-bed reactor in a stainless steel tube with a length of 330 mm and an inner diameter of 12 mm at normal pressure and various temperatures. Briefly, 0.5 g catalyst was mixed with an equivalent weight of quartz sand (40–70 mesh) and reduced in situ under pure H_2 with a gas hourly space velocity (GHSV) of 2000 mL g^{-1} h^{-1} at 500 °C for 9 hours before the catalytic test. Then the instrument was cooled to 160 °C and a mixed stream of CO_2 and H_2 (volumetric ratio of H_2/CO_2 = 4) was introduced into the gas circuit as the feedstock. The gases in the outflow were analysed using an online gas chromatograph (Fuli 9790II). CH_4 (S_{CH_4}) selectivity and CO_2 (X_{CO_2}) conversion were determined by the following equations:

$$X_{CO_2} = \frac{W_{CO_2,in} - W_{CO_2,out}}{W_{CO_2,in}} \times 100\% \qquad (1)$$

$$S_{CH_4} = \frac{W_{CH_4,out}}{W_{CH_4,out} + W_{CO,out}} \times 100\% \qquad (2)$$

where, $W_{CO_2,in}$ denotes the moles of CO_2 in the feedstock, and $W_{CO_2,out}$, $W_{CO,out}$, and $W_{CH_4,out}$ denote the carbon moles of CO_2, CO and CH_4 at the outflow reactor, respectively.

3 Results and discussion

3.1 Characterization of the catalysts

The X-ray powder diffraction (PXRD) patterns of fresh Ni/Al_2O_3–CeO_2-x (x = 10, 5.0, 2.5, and 1.0) samples are shown in Fig. 1. In the pattern of the Ni/Al_2O_3 catalyst, we could observe a broad peak from 29.9 to 45.9°, which was assigned to the amorphous phase of Al_2O_3. Four new diffraction peaks at 33.3°, 38.6°, 55.8° and 66.5° appeared after the introduction of the Ce species, which corresponded to the characteristic peaks of CeO_2. In general, a higher Ce loading in the composite resulted in an increased degree of crystallization of Al_2O_3, as confirmed by the gradual narrowing of the broad peak (Fig. 1). Meanwhile, no obvious characteristic diffraction peaks of bulk NiO could be detected in the Ni/Al_2O_3–CeO_2-x composites, suggesting an amorphous form and an even distribution of Ni-based materials on the surface of the Al_2O_3–CeO_2 composites, as expected.

The influence of the presence of cerium and nickel on the Brunauer–Emmett–Teller (BET) pore size distributions and specific surface areas of the Ni/Al_2O_3–CeO_2 composites with

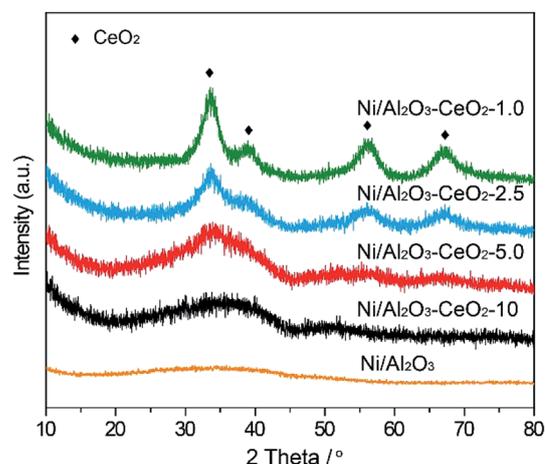**Fig. 1** PXRD patterns of the fresh Ni/Al_2O_3–CeO_2-x catalysts.

Paper

RSC Advances

different molar ratios of Al/Ce were evaluated by N_2 sorption isotherms at 77 K (Fig. 2). Similar to the single Ni–Al_2O_3 sample, all the Ni/Al_2O_3–CeO_2 composites displayed type IV isotherms with big hysteresis loops, demonstrating the existence of mesopores in these composite supports. The pristine mesoporous Al_2O_3-modified Ni catalyst had a high specific surface area of 291 m^2 g^{-1} with an average pore volume of 0.35 cm^3 g^{-1}. As the Ce loading in the Ni/Al_2O_3–CeO_2-x composites was increased, the region of the hysteresis loops tended to decrease (Fig. 2A); at the same time, the average pore diameters widened gradually in the range 3.66 to 4.35 nm (Fig. 2B), indicating that the Ce and Ni species might occupy the small pores of Al_2O_3 or cause partial collapse of pristine structures. The basic data on the catalysts are listed in Table S1.† The prepared Ni/Al_2O_3–CeO_2-x samples exhibited obvious decreases in pore volumes and specific surface areas, but an increase in pore diameters in comparison to the Ni/Al_2O_3 catalyst. These results may be ascribed to the covering of the Al_2O_3 surface by Ce or Ni species, or the aggregation of NiO species.

3.2 Effect of Ce content

H_2-TPR was used to test the reduction behaviour of the Ni/Al_2O_3–CeO_2-x catalysts (Fig. 3), and the Ni/Al_2O_3 catalyst was also measured for comparison. The Ce content had a remarkable effect on the reduction of Ni^{2+} ions in the composites. With increasing amounts of Ce in the Ni/Al_2O_3–CeO_2 composites, the reduction peaks for the NiO species shifted gradually to lower temperatures (624 °C for Ni/Al_2O_3 to 504 °C for Ni/Al_2O_3–CeO_2-1.0). This indicated that the doping of cerium into the Ni/Al_2O_3–CeO_2 supports broke the reciprocities between Al_2O_3 and NiO due to the formation of the Al_2O_3–CeO_2 composite, which was beneficial for the reduction of NiO. The reduction peak at around 624 °C could be observed for the Ni/Al_2O_3 sample; the high temperature could be ascribed to the intense interactions between the Al_2O_3 support and NiO species. For Ce-doped samples, the reduction peaks for Ni/Al_2O_3–CeO_2-x shifted slowly to lower temperature with increasing Ce loading, and the consumption of H_2 also increased, which could be attributed to the Ce^{3+}/Ce^{4+} couple, which could create both bulk and surface
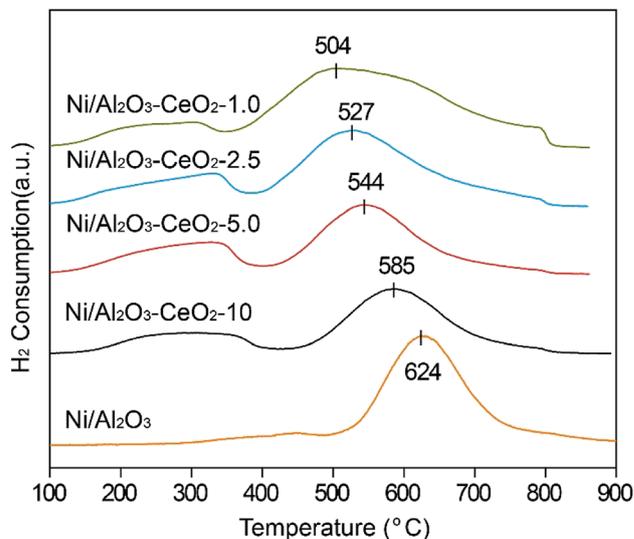

Fig. 3 H_2-TPR profiles of the fresh Ni/Al_2O_3–CeO_2-x catalysts.

oxygen vacancies.[35] The inferior reduction behaviour of the Ni-based species on mesoporous Al_2O_3 led to inadequate numbers of active metallic Ni sites in comparison with those in the Ni-supported Al_2O_3–CeO_2 composites. The best reduction behaviour of NiO species in this study was obtained for the catalyst with the Al/Ce molar ratio of 1.0.

The valence state of Ni, the interactions between NiO species and the Al_2O_3–CeO_2 support, and the surface chemical environment of fresh Ni/Al_2O_3–CeO_2-x catalysts were further revealed by XPS (Fig. 4). The binding energy at 855.9 eV of Ni $2p_{3/2}$ is the characteristic peak of Ni^{2+}, and no obvious peak shift could be detected for Ni/Al_2O_3–CeO_2-x regardless of the Al/Ce ratio (Fig. 4A), which demonstrated that the Ce content did not change the chemical environment of the NiO species dispersed on the surface of the composites. From this observation in combination with the PXRD analysis, we could infer that the nickel existed on the surface of the catalyst mainly as highly dispersed NiO species. However, the intensity of the Ni^{2+} peak strengthened with increasing Ce content, indicating the
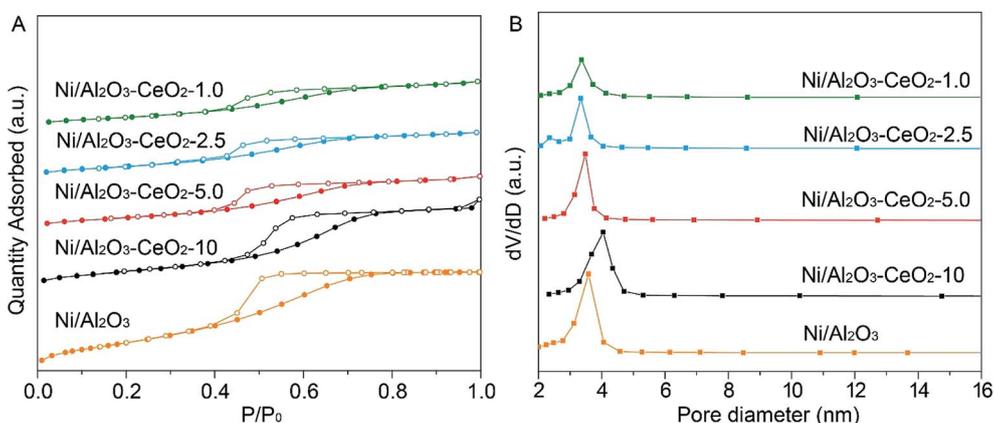

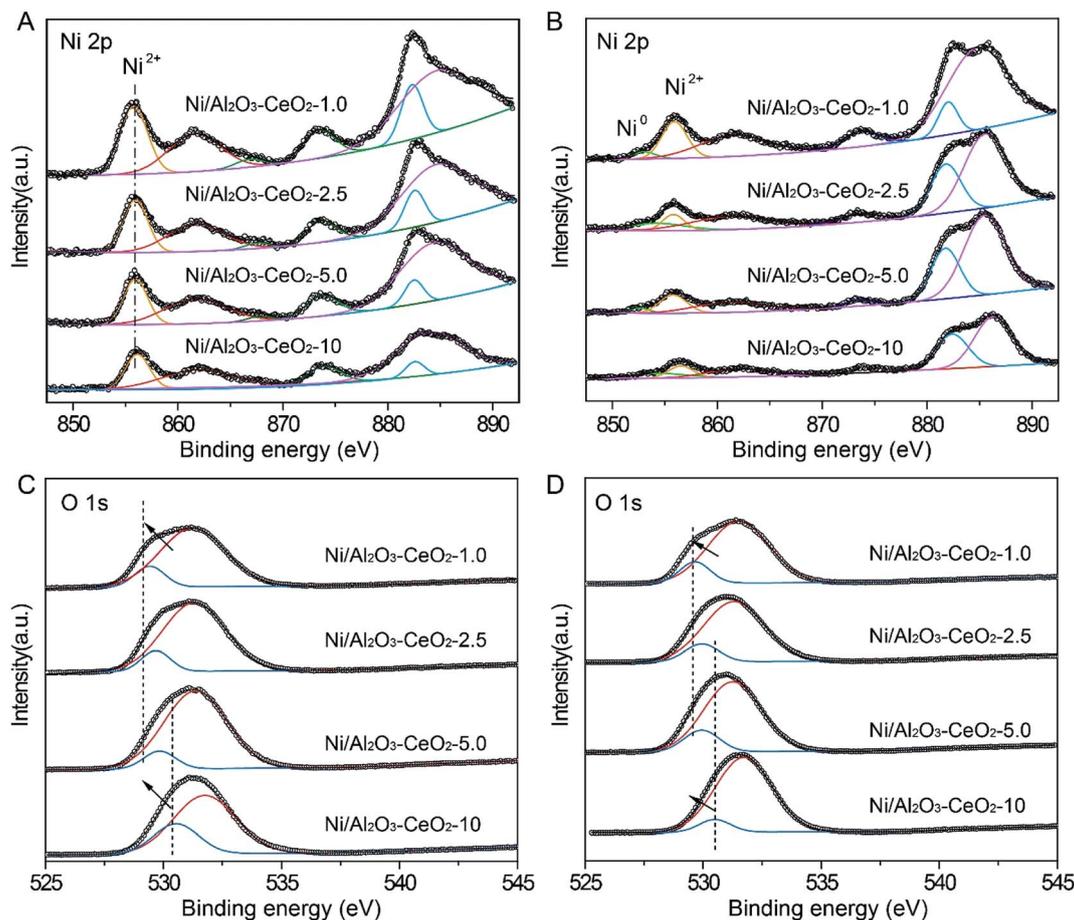**Fig. 2** (A) N_2 adsorption–desorption isotherms and (B) BJH pore size distributions of the fresh Ni/Al_2O_3–CeO_2-x catalysts.

Fig. 4 XPS spectra for (A) fresh and (B) spent Ni/Al$_2$O$_3$–CeO$_2$-x catalysts in the Ni 2p region, and (C) fresh and (D) spent Ni/Al$_2$O$_3$–CeO$_2$-x catalysts in the O 1s region.

generation of vast numbers of active sites on the support surface in the reduction process, which could be further confirmed by the XPS of spent catalysts (Fig. 4B). The XPS peak at around 529.9 eV corresponded to the lattice oxygen (OL) on the surface of CeO$_2$ or Al$_2$O$_3$ (Fig. 4C and D), and another peak at around 530.9 eV was assigned to adsorbed oxygen (OA) on the surface.[36] The detailed information about the OA to OL ratio for the fresh composites on the basis of the OL and OA area percentages is summarized in Table S2.† The OA and OL peaks for the Ni-supported Al$_2$O$_3$–CeO$_2$ catalysts were located in the ranges 531.2–531.9 eV and 529.6–531.0 eV, respectively. With increasing Ce content, the peaks shifted slowly to lower binding energies, which may be ascribed to the ever-increasing numbers of oxygen vacancies on the surface of the Al$_2$O$_3$–CeO$_2$ catalysts at higher Ce content, thus contributing to the adsorption and conversion of CO$_2$ by the catalysts.[37]

3.3 Catalytic performance

The catalytic hydrogenation of CO$_2$ to CH$_4$ with the Ni/Al$_2$O$_3$–CeO$_2$-x catalysts was performed in a fixed-bed reactor (GHSV of 6000 mL g^{-1} h^{-1}, H$_2$/CO$_2$ = 4.0, atmospheric pressure, temperature varied from 150 to 450 °C). As the reaction temperature was progressively increased, the CO$_2$ conversion

first increased for all catalysts, but it then reached a peak value at an optimum reaction temperature and started to decrease (Fig. 5A). The catalytic activity declined when the temperature was further increased to 350 °C, which could be ascribed to the endothermic reverse reaction. The CeO$_2$-modified catalysts displayed an obviously higher CH$_4$ selectivity compared with the single Ni/Al$_2$O$_3$ sample (Fig. 5B). The amount of CeO$_2$ in the Al$_2$O$_3$–CeO$_2$ composite had a critical impact on the catalytic performance, especially at lower temperature. The Ni/Al$_2$O$_3$ catalyst without CeO$_2$ displayed a low CO$_2$ conversion of only 9.8% at the low reaction temperature of 250 °C, but when we introduced trace amounts of Ce species into the catalyst (Ni/Al$_2$O$_3$–CeO$_2$-10), the conversion of CO$_2$ increased sharply to the value of 42.9%. It was noteworthy that the CO$_2$ conversion increased step-by-step when the CeO$_2$ loading was increased in the Ni-modified Al$_2$O$_3$–CeO$_2$ samples. Apparently, with an increase of CeO$_2$ content, a lower temperature was sufficient to reach the same CO$_2$ conversion level; the excellent catalytic performance of 78% CO$_2$ conversion with 100% CH$_4$ selectivity was obtained for the Ni/Al$_2$O$_3$–CeO$_2$-1.0 composite catalyst at the relatively low temperature of 320 °C.

In order to investigate the effect of Ce species on the long-term durability of the catalyst, measurements were performed
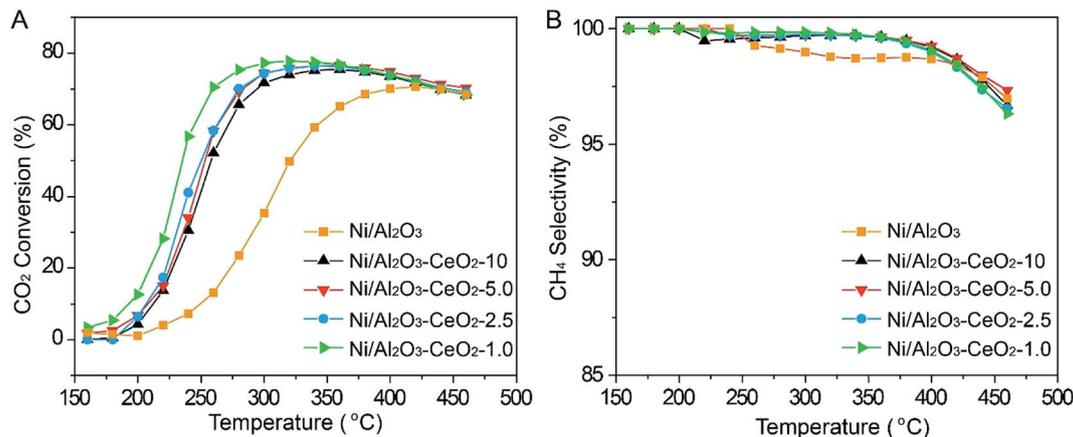
Fig. 5 (A) CO_2 conversion and (B) CH_4 selectivity of the Ni/Al_2O_3–CeO_2-x catalysts. GHSV = 6000 mL g^{-1} h^{-1}, P = 0.1 MPa, H_2/CO_2 = 4.

over a time period of 100 h for the Ni/Al_2O_3–CeO_2-1.0 catalyst (Fig. 6). Indeed, the loading of CeO_2 in the composite had a significant influence on the catalytic performance of CO_2 methanation. The Ni/Al_2O_3–CeO_2-1.0 sample exhibited 78% CO_2 conversion with almost 100% CH_4 selectivity during the 100 h test, demonstrating excellent long-term stability and selectivity, and showing that CeO_2 doping significantly improved the long-term stability of Ni/Al_2O_3 catalysts. Obviously, the introduction of CeO_2 could promote catalytic stability and activity at the same time, which may be attributed to the generation of oxygen vacancies on the surface of the support and the increased metallic nickel surface area, as evidenced by XPS (Fig. 4C and D). On the one hand, Ni species provided active sites for activating molecular CO_2 and could facilitate the formation of atomic hydrogen by dissociating H_2 from the Ni-based catalyst. On the other hand, the surface oxygen vacancies resulted in the formation of carbon species, which could react with the atomic hydrogen on the surface of the catalyst to form CH_4. The structural stability of the Ni/Al_2O_3–CeO_2-1.0 catalyst was further confirmed by PXRD after the long-term

reaction; no obvious change could be observed when it was compared with the fresh catalyst (Fig. S1†).

4 Conclusions

To sum up, Ni-modified mesoporous Al_2O_3–CeO_2 composite catalysts containing various amounts of CeO_2 were synthesized through a one-pot sol–gel route and used for CO_2 conversion to CH_4 at low reaction temperatures. The mesoporous Ni/Al_2O_3–CeO_2 catalysts displayed excellent CH_4 selectivity and CO_2 conversion in comparison to the single Ni-modified Al_2O_3 catalyst. The uniform distribution of Ni species combined with the improved surface oxygen vacancies resulting from CeO_2 loading on the support made the excellent catalytic activity and CH_4 selectivity possible at lower temperatures. The Ni/Al_2O_3–CeO_2-1.0 catalyst displayed impressive catalytic properties of 78% CO_2 conversion with 100% CH_4 selectivity at 320 °C; this performance was retained without any decay during 100 h of testing.

Conflicts of interest

There are no conflicts to declare.

Acknowledgements

Fig. 6 Stability tests on the Ni/Al_2O_3–CeO_2-1.0 catalyst at 320 °C, GHSV = 6000 mL g^{-1} h^{-1}, P = 0.1 MPa, H_2/CO_2 = 4.

References

1 W. Wang, S. Wang, X. Ma and J. Gong, *Chem. Soc. Rev.*, 2011, **40**, 3703–3727.

2 M. Gassner and F. Marechal, *Energy Environ. Sci.*, 2012, **5**, 5768–5789.

3 C. Janke, M. S. Duyar, M. Hoskins and R. Farrauto, *Appl. Catal. B Environ.*, 2014, **152–153**, 184–191.

4 I. Dimitriou, P. García-Gutiérrez, R. H. Elder, R. M. Cuéllar-Franca, A. Azapagic and R. W. K. Allen, *Energy Environ. Sci.*, 2015, **8**, 1775–1789.

5 K. Mueller, M. Staedter, F. Rachow, D. Hoffmannbeck and D. Schmeisser, *Environ. Earth Sci.*, 2013, **70**, 3771–3778.

6 M. Younas, L. Loong Kong, M. J. K. Bashir, H. Nadeem, A. Shehzad and S. Sethupathi, *Energy Fuels*, 2016, **30**, 8815–8831.

7 P. Frontera, A. Macario, M. Ferraro and P. Antonucci, *Catalysts*, 2017, **7**, 59.

8 J. Gao, Q. Liu, F. Gu, B. Liu, Z. Zhong and F. Su, *RSC Adv.*, 2015, **5**, 22759–22776.

9 M. A. A. Aziz, A. A. Jalil, S. Triwahyono and A. Ahma, *Green Chem.*, 2015, **17**, 2647–2663.

10 Y. Zhu, S. Zhang, Y. Ye, X. Zhang, L. Wang, W. Zhu, F. Chang and F. Tao, *ACS Catal.*, 2012, **2**, 2403–2408.

11 A. Karelovic and P. Ruiz, *ACS Catal.*, 2013, **3**, 2799–2812.

12 M. Younas, L. L. Loong, M. J. K. Bashir, H. Nadeem, A. Shehzad and S. Sethupathi, *Energy Fuels*, 2016, **30**, 8815–8831.

13 S. He, C. Li, H. Chen, D. Su, B. Zhang, X. Cao, B. Wang, M. Wei, D. G. Evans and X. Duan, *Chem. Mater.*, 2013, **25**, 1040–1046.

14 G. A. Du, S. Y. Lim, Y. H. Yang, C. Wang, L. Pfefferle and G. L. Haller, *J. Catal.*, 2007, **249**, 370–379.

15 D. Wierzbicki, R. Debek, M. Motak, T. Grzybek, M. E. Gálvez and P. Da Costa, *Catal. Commun.*, 2016, **83**, 5–8.

16 S. Rahmani, M. Rezaei and F. Meshkani, *J. Ind. Eng. Chem.*, 2014, **20**, 346–352.

17 D. Wierzbicki, R. Baran, R. Dębek, M. Motak, M. E. Gálvez, T. Grzybek, P. Da Costa and P. Glatzel, *Appl. Catal. B Environ.*, 2018, **232**, 409–419.

18 X. Zou, X. Wang, L. Li, K. Shen, X. Lu and W. Ding, *Int. J. Hydrogen Energy*, 2010, **35**, 13191–13200.

19 W. Wang and J. Gong, *Front. Chem. Sci. Eng.*, 2011, **5**, 2–10.

20 C. Cheng, D. Shen, R. Xiao and C. Wu, *Fuel*, 2017, **189**, 419–427.

21 T. A. Le, M. S. Kim, S. H. Lee, T. W. Kim and E. D. Park, *Catal. Today*, 2017, **293–294**, 89–96.

22 G. Zhou, H. Liu, K. Cui, H. Xie, Z. Jiao, G. Zhang, K. Xiong and X. Zheng, *Int. J. Hydrogen Energy*, 2017, **42**, 16108–16117.

23 J. Lin, C. Ma, J. Luo, X. Kong, Y. Xu, G. Ma, J. Wang, C. Zhang, Z. Li and M. Ding, *RSC Adv.*, 2019, **9**, 8684–8694.

24 Y. Yan, Y. Dai, H. He, Y. Yu and Y. Yang, *Appl. Catal. B Environ.*, 2016, **196**, 108–116.

25 K. M. Lee and W. Y. Lee, *Catal. Lett.*, 2002, **83**, 65–70.

26 M. Romero-Sáez, A. B. Dongil, N. Benito, R. Espinoza-González, N. Escalona and F. Gracia, *Appl. Catal. B Environ.*, 2018, **237**, 817–825.

27 J. Lin, C. Ma, Q. Wang, F. Xu, G. Ma, J. Wang, H. Wang, C. Dong, C. Zhang and M. Ding, *Appl. Catal. B Environ.*, 2019, **243**, 262–272.

28 Y. Lu, S. Li and L. Guo, *Fuel*, 2013, **103**, 193–199.

29 L. Zhou, Q. Wang, L. Ma, J. Chen, J. Ma and Z. Zi, *Catal. Lett.*, 2015, **145**, 612–619.

30 M. Ding, J. Tu, Q. Zhang, M. Wang, N. Tsubaki, T. Wang and L. Ma, *Biomass Bioenergy*, 2016, **85**, 12–17.

31 J. Chen, R. Wang, J. Zhang, F. He and S. Han, *J. Mol. Catal. A: Chem.*, 2005, **235**, 302–310.

32 M. M. Barroso-Quiroga and A. E. Castro-Luna, *Int. J. Hydrogen Energy*, 2010, **35**, 6052–6056.

33 L. Zhou, Q. Wang, L. Ma, J. Chen, J. Ma and Z. Zi, *Catal. Lett.*, 2015, **145**, 612–619.

34 D. Chen, D. He, J. Lu, L. Zhong, F. Liu, J. Liu, J. Yu, G. Wan, S. He and Y. Luo, *Appl. Catal. B Environ.*, 2017, **218**, 249–259.

35 H. Liu, X. Zou, X. Wang, X. Lu and W. Ding, *J. Nat. Gas Chem.*, 2012, **21**, 703–707.

36 W. Zheng, J. Zhang, Q. Ge, H. Xu and W. Li, *Appl. Catal. B Environ.*, 2008, **80**, 98–105.

37 W. Nie, X. Zou, X. Shang, X. Wang, W. Ding and X. Lu, *Fuel*, 2017, **202**, 135–143.